

# A Search For The Higgs Boson In $H \rightarrow ZZ \rightarrow 2\ell 2\nu$ Mode

D. Trocino

Department of Physics, Northeastern University, Boston, MA, USA

A search for the Standard Model Higgs boson in proton-proton collisions at a center-of-mass energy of 7 TeV is presented in the decay channel  $H \rightarrow ZZ \rightarrow 2\ell 2\nu$ . The search is conducted by the CMS experiment with data accumulated during the 2010 and part of the 2011 running periods of the LHC, for a total integrated luminosity of  $1.1 \text{ fb}^{-1}$ . No excess is observed in the  $ZZ$  transverse mass. Limits are set on the production of the Higgs boson in the context of the Standard Model and in the presence of a sequential fourth family of fermions with high masses.

## 1. Introduction

The search for the Higgs boson and its discovery are among the central goals of the experiments at the LHC. Direct searches at the LEP collider have set a lower limit on the Standard Model (SM) Higgs mass of  $114 \text{ GeV}/c^2$  [1], while direct searches at the Tevatron exclude the SM Higgs in the mass range  $158\text{-}173 \text{ GeV}/c^2$  at 95% confidence level [2]. The primary production mechanism for the Higgs at the LHC is gluon-gluon fusion, with a small contribution from vector boson fusion [4].

In the following, a search for the SM Higgs boson in the  $H \rightarrow ZZ \rightarrow 2\ell 2\nu$  channel is presented [3]. This channel is especially suited for high-mass Higgs boson searches, and a mass range from 250 to  $600 \text{ GeV}/c^2$  is considered in this analysis. Results are reported based on a data sample corresponding to an integrated luminosity of  $1.1 \text{ fb}^{-1}$ , recorded by the CMS experiment at the LHC at a center-of-mass energy of 7 TeV. An interpretation of the results in terms of exclusion limits for the Higgs boson is also presented in a scenario with a fourth generation of fermions [5] added to the SM. For sufficiently large lepton and quark masses, this SM extension has not been excluded by existing constraints [6]. Here we consider a fourth generation mass of  $600 \text{ GeV}/c^2$ .

## 2. The CMS Detector

The innermost component of the CMS detector is the tracking system, equipped with silicon pixel and microstrip detectors, used to measure the momenta of charged particles and reconstruct the interaction vertices. The tracker is immersed in a solenoidal magnetic field of 3.8 T and covers the pseudorapidity range  $|\eta| < 2.5$ .

The tracker is surrounded by an electromagnetic calorimeter (ECAL), made of  $\text{PbWO}_4$  crystals, and a brass/scintillating fiber hadronic calorimeter (HCAL). Both calorimeters cover the pseudorapidity range  $|\eta| < 3.0$ . To improve the detector hermeticity, forward quartz-fiber Cherenkov calorimeters (HF) extend the coverage up to  $|\eta| = 5.0$ .

The outermost part of the CMS detector is the muon spectrometer, used to measure the momentum of muons traversing through the detector. It consists of three different types of gaseous detectors embedded in the iron return yoke: drift tube chambers (DT) in the barrel, cathode strip chambers (CSC) in the endcaps, and resistive plate chambers (RPC) in both regions.

A detailed description of the CMS detector can be found in [7].

## 3. Simulation of Physics Processes

In this analysis, signal and background datasets are produced by detailed Monte Carlo simulation of the detector response, based on GEANT4 [7, 8], taking into account the limited inter-calibration and alignment precision, and using the full CMS reconstruction chain.

The  $H \rightarrow ZZ \rightarrow 2\ell 2\nu$  signal and the Drell-Yan and  $t\bar{t}$  backgrounds are generated using the program POWHEG [9]. The  $W + \text{jets}$  and single top events are simulated using MADGRAPH [10], while the diboson backgrounds ( $ZZ, WZ, WW$ ) are simulated using PYTHIA [11]. In case of the irreducible  $ZZ$  background, a dynamic next-to-leading order  $k$ -factor is applied as a function of the transverse momentum of the  $Z$  boson (see Fig. 1, *left*). This  $k$ -factor has been computed using the MCFM program [12]. Contributions from the  $gg \rightarrow ZZ$  events are also taken into account [13] (see Fig. 1, *right*).

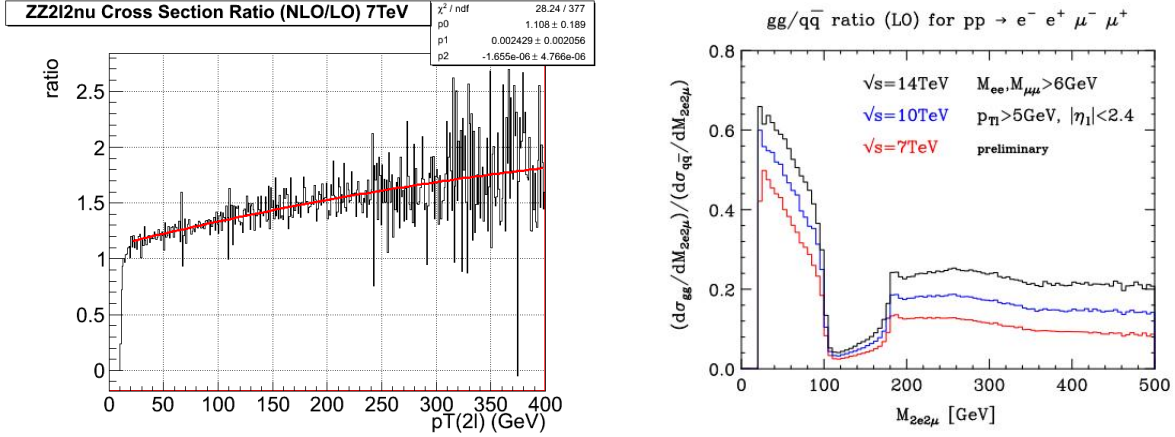


Figure 1: *left*: NLO to LO cross section ratio for  $ZZ \rightarrow 2\ell 2\nu$  at  $\sqrt{s} = 7$  TeV as a function of the dilepton transverse momentum, computed using MCFM; *right*: contribution of the  $gg \rightarrow ZZ$  subprocess relative to  $qq \rightarrow ZZ$  contribution.

## 4. Event selection

If the mass of the Higgs boson is much larger than twice the mass of the  $Z$  boson, each  $Z$  boson produced in the Higgs boson decay has a significant transverse momentum ( $p_T$ ). Consequently, a  $H \rightarrow ZZ \rightarrow 2\ell 2\nu$  event is characterized by the presence of a boosted pair of isolated leptons,  $e^+e^-$  or  $\mu^+\mu^-$ , with invariant mass consistent with the  $Z$  mass, and large missing transverse energy (MET) arising from the decay of the other  $Z$  boson into neutrinos.

### 4.1. Trigger and Preliminary Selections

Since the final state involves two high- $p_T$  isolated leptons, events selected for the analysis are required to pass dilepton triggers. In case of the muon channel, a trigger with a threshold of  $p_T > 7$  GeV/ $c$  for each muon was used in the initial data-taking period (about  $191 \text{ pb}^{-1}$ ), while for the remainder of the dataset the thresholds were 13 and 8 GeV/ $c$  for the leading and second muon, respectively. The efficiency for selecting signal events with these dimuon triggers is found to vary between 95 and 99%, depending on the transverse momentum and pseudorapidity of the muons. In case of the electron channel, the trigger has thresholds of  $p_T > 17$  GeV/ $c$  on the leading electron and  $p_T > 8$  GeV/ $c$  on the second electron. The efficiency for this trigger is found to be larger than 99%.

In order to suppress events with an incorrect MET measurement due to detector noise, a filter is applied to remove events in which anomalous HCAL noise is detected. Beam-halo events are also vetoed.

An event is required to have at least one primary vertex within 24 cm of the geometrical center of the CMS detector in the beam direction and within 0.2 cm in the plane transverse to the beam. In events with multiple vertices, the one with the largest value of  $\sum p_T^2$  for the associated tracks is chosen as the reference vertex.

### 4.2. Lepton and Dilepton Selection

Muon candidates can be reconstructed using two algorithms: one uses tracks in the inner silicon tracker matched to segments in the muon system; the other algorithm uses tracks produced from a global fit of tracker and muon chamber hits, seeded by segments in the muon system [14]. Further identification criteria based on the number of hits in the tracker and the muon system, the fit quality of the muon track and its consistency with the primary vertex, are imposed on the muon candidates to reduce fakes.

Electron reconstruction also involves two algorithms, one in which energy clusters in the ECAL are matched to hits in the silicon tracker, and another in which tracks in the silicon tracker are matched to the ECAL clusters [15]. These reconstructed electrons are required to pass further identification criteria, based on the ECAL shower shape, track-ECAL cluster matching, and consistency with the primary vertex. Additional requirements are imposed to remove electrons produced in photon conversions.

To further suppress the QCD background, leptons are required to be isolated: a cone of radius  $\Delta R = \sqrt{\Delta\phi^2 + \Delta\eta^2} = 0.3$  is defined around the leptons, and the sum of transverse energy deposits in the calorimeters

and the transverse momenta of tracks in this cone is computed. This isolation sum is required to be smaller than 15% (10%) of the momentum of the muon (electron). The median energy expected from pileup interactions is subtracted from the isolation sum, in order to reduce possible inefficiencies from enhanced detector activity in events with high pileup [16].

Events are selected such that there are two well-identified, isolated, opposite-charge leptons of the same flavor, each with  $p_T > 20$  GeV/ $c$ , which form an invariant mass consistent with the  $Z$  mass. In addition, events are required to have exactly two leptons with  $p_T > 10$  GeV/ $c$ : events with any additional lepton are rejected in order to reduce the  $WZ$  background in which the  $W$  and  $Z$  bosons both decay leptonically. Moreover, the dilepton candidate is required to have a transverse momentum larger than 25 GeV/ $c$ . The impact of this cut on signal efficiency is small (less than 1% for all the Higgs boson masses considered), but allows the use of  $\gamma +$  jets data to effectively model the  $Z +$  jets background, as explained in the following.

With this selection, the principal backgrounds in this analysis are  $Z +$  jets,  $t\bar{t}$ , single top,  $W +$  jets,  $WZ$ ,  $WW$ , and  $ZZ$  events.

### 4.3. B-Tag Veto

In order to suppress backgrounds containing top quarks (single top,  $t\bar{t}$ ), events with at least one  $b$ -tagged jet are vetoed. Particle Flow jets [17] with a transverse energy  $E_T > 30$  GeV are considered for  $b$ -tagging.  $B$ -jets are tagged using the ‘‘Track Counting High Efficiency’’ (TCHE) algorithm [18], which uses displaced tracks in a jet to compute a  $b$ -tagging discriminator.

### 4.4. Missing Transverse Energy

The signal process  $H \rightarrow ZZ \rightarrow 2\ell 2\nu$  is characterized by a large missing  $E_T$ , arising from the two neutrinos in the final state. Therefore, a high threshold is imposed on the Particle Flow MET [19] in order to suppress the large Drell-Yan background, which is characterized by little real missing transverse energy. However, jet mismeasurements and detector effects can produce large MET values in  $Z +$  jets events. Since this background is five orders of magnitude more abundant than the signal, the contamination of the selected signal region due to the high-MET tail is very significant. To further suppress backgrounds with fake MET coming from jet mismeasurements, events in which the MET is aligned with a jet are removed using a cut on the  $\Delta\phi(\text{MET}, \text{jet})$  variable. Both the MET threshold and the  $\Delta\phi$  cut are dependent on the Higgs mass hypothesis, since high-mass Higgs events are characterized by larger MET.

### 4.5. Transverse Mass

Higgs signal events show a narrower transverse mass distribution than background events, where the Higgs transverse mass is defined as

$$M_T^2 = \left( \sqrt{p_{T,Z}^2 + M_Z^2} + \sqrt{\text{MET}^2 + M_Z^2} \right)^2 - \left( p_{T,Z} + \vec{\text{MET}} \right)^2.$$

An  $m_H$ -dependent two-sided cut is thus applied to the  $M_T$  variable to further separate signal from background.

The event selection criteria used in the analysis are listed in Table I. For MET,  $\Delta\phi(\text{MET}, \text{jet})$  and  $M_T$  cuts, which are smoothly dependent on the Higgs mass, thresholds for selected mass points are shown as examples.

## 5. Background Estimation

All the backgrounds in this analysis can be divided into three categories:

- $Z +$  jets with fake MET due to jet mismeasurement and detector effects;
- non-resonant backgrounds (i.e., events without a  $Z$  resonance):  $t\bar{t}$ , single top,  $WW$ ,  $W +$  jets;
- irreducible background: electroweak  $ZZ$  pair production and fully leptonic decays of  $WZ$  pairs.

$ZZ$  and  $WZ$  backgrounds are modeled using simulation, while the remaining backgrounds ( $Z +$  jets and all non-resonant ones) are estimated using data-driven methods.

Table I: Event selection cuts.

Cut	Cut Value
Lepton transverse momenta	$p_T > 20 \text{ GeV}/c$
$Z$ mass window	$ m_{\ell\ell} - 91.1876 \text{ GeV}/c^2  \leq 15 \text{ GeV}/c^2$
Transverse momentum of vetoed 3 <sup>rd</sup> lepton	$p_T > 10 \text{ GeV}/c$
$Z$ transverse momentum	$p_{T,Z} > 25 \text{ GeV}/c$
$b$ -tag veto (jet $p_T > 30 \text{ GeV}/c$ )	TCHE discriminator $< 2$
MET-jet separation	$m_H = 250 \text{ GeV}/c^2$ : $\Delta\phi(\text{MET}, \text{jet}) > 0.62 \text{ rad}$ $m_H = 350 \text{ GeV}/c^2$ : $\Delta\phi(\text{MET}, \text{jet}) > 0.14 \text{ rad}$ $m_H = 500 \text{ GeV}/c^2$ : —
Missing transverse energy (MET)	$m_H = 250 \text{ GeV}/c^2$ : MET $> 69 \text{ GeV}$ $m_H = 350 \text{ GeV}/c^2$ : MET $> 97 \text{ GeV}$ $m_H = 500 \text{ GeV}/c^2$ : MET $> 141 \text{ GeV}$
Transverse mass ( $M_T$ )	$m_H = 250 \text{ GeV}/c^2$ : $216 \text{ GeV}/c^2 > M_T > 272 \text{ GeV}/c^2$ $m_H = 350 \text{ GeV}/c^2$ : $267 \text{ GeV}/c^2 > M_T > 386 \text{ GeV}/c^2$ $m_H = 500 \text{ GeV}/c^2$ : $M_T > 336 \text{ GeV}/c^2$

## 5.1. $Z$ + jets Estimation

The photon + jets process is very similar to  $Z$  + jets in terms of generating fake MET from mismeasured jets. Moreover, the cross section for  $\gamma$  + jets events is much greater than that of  $Z$  + jets. The former process can thus be used to build a model of the latter, provided that the two samples can be made kinematically identical. This is achieved by reweighting the  $\gamma$  + jets events so that the  $p_T$  spectrum of the photon matches the observed dilepton  $p_T$  spectrum. An additional reweighting is applied to match the jet multiplicity between the two samples. The photon is also assigned a random mass, according to the  $Z$  lineshape observed in dilepton events, and the yield of the photon sample is normalized to that of the  $Z$ . Lastly, the full analysis selection is applied to the reweighted photon sample. The MET distribution obtained with this procedure models very accurately the spectrum observed in Drell-Yan events (see Fig. 2). The statistical error for the  $Z$  + jets prediction thus obtained is computed by summing in quadrature the weights of the  $\gamma$  + jets events.

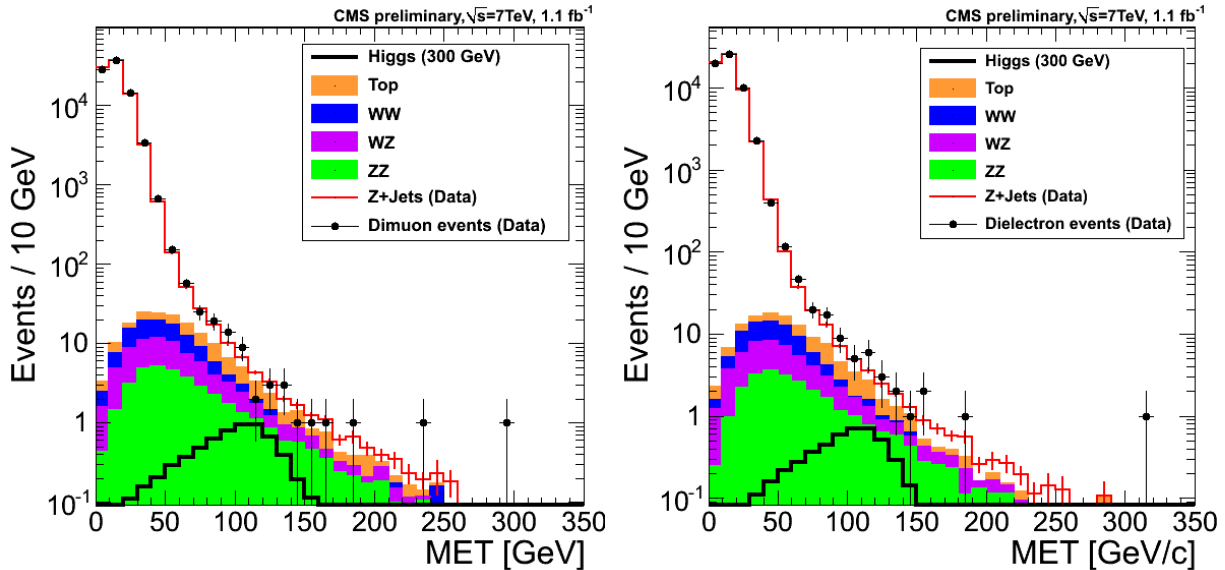


Figure 2: MET spectrum of dimuon events (*left*) and dielectron events (*right*), compared with reweighted single photon events in  $1.1 \text{ fb}^{-1}$  of data.

## 5.2. Non-Resonant Background Estimation

The non-resonant backgrounds consist of several contributions. Events with  $t\bar{t}$  and  $WW$  are characterized by a final state with two prompt leptons from  $W$  decays and real MET, plus two  $b$ -jets for  $t\bar{t}$ . Single top events produced in the most common  $tW$ -channel show a similar signature.  $W$  + jets has instead one prompt lepton and a jet faking a second lepton.

All non-resonant backgrounds can be estimated using events with a final state containing  $e^+\mu^-$  or  $e^-\mu^+$  pairs and passing the full analysis selection. The background level in the  $e^+e^-$  and  $\mu^+\mu^-$  final states is computed using the relations  $N_{\mu\mu} = \alpha_\mu \times N_{e\mu}$  and  $N_{ee} = \alpha_e \times N_{e\mu}$ , where the scale factors  $\alpha$  can be computed from the sidebands (SB) of the  $Z$  peak:

$$\alpha_\mu = \frac{N_{\mu\mu}^{SB}}{N_{e\mu}^{SB}}, \quad \alpha_e = \frac{N_{ee}^{SB}}{N_{e\mu}^{SB}}.$$

This method cannot distinguish between the non-resonant background and the signal in the  $H \rightarrow WW \rightarrow 2l2\nu$  channel. Such signal events are therefore treated as a part of the background estimate. This signal contamination is found to be less than 7% of the total background yield for all considered Higgs masses. In the SM scenario with a fourth generation of fermions, this contamination increases, up to about 50% of the total background for a Higgs mass of 250 GeV/ $c^2$ . Table II lists the predicted yields for non-resonant backgrounds with 1.1 fb $^{-1}$ .

Table II: Yields from 1.1 fb $^{-1}$  data for non-resonant backgrounds in the muon (*left*) and electron (*right*) channels. Statistical uncertainties are also quoted.

$m_H$	Predicted Yields	MC Prediction	$m_H$	Predicted Yields	MC Prediction
250	$13 \pm 3$	$12 \pm 0.65$	250	$9.4 \pm 2.2$	$9.5 \pm 0.61$
300	$3 \pm 1.4$	$4.8 \pm 0.39$	300	$2.2 \pm 1$	$3.7 \pm 0.36$
350	$2 \pm 1.2$	$1.4 \pm 0.21$	350	$1.3 \pm 0.78$	$0.99 \pm 0.16$
400	$0.68 \pm 0.69$	$0.42 \pm 0.11$	400	$0.5 \pm 0.5$	$0.36 \pm 0.1$
500	0	$0.038 \pm 0.033$	500	0	$0.17 \pm 0.075$
600	0	0	600	0	0

## 6. Systematic Uncertainties

The signal and background yields are subject to several systematic uncertainties, summarized in Table III. Most of these uncertainties apply to processes derived from simulation (Higgs signal,  $ZZ$  and  $WZ$  backgrounds) or to data-driven estimates of backgrounds ( $Z$  + jets and non-resonant backgrounds.)

## 7. Results and Conclusions

Figure 3 shows the  $M_T$  distributions of the selected dilepton events from data and the estimated background for the 250 GeV/ $c^2$  and 350 GeV/ $c^2$  Higgs mass hypotheses. No evidence of Higgs boson production is found. Table IV lists the event yields after the full selection for various Higgs mass hypotheses, for the estimated backgrounds, and for the 1.1 fb $^{-1}$  dataset.

Figure 4 (*left*) shows the 95% mean expected and observed C.L. upper limits on  $\sigma \times BR(H \rightarrow ZZ \rightarrow 2\ell 2\nu)$  (*above*), and the ratio  $R$  of such limit to the SM cross section  $\sigma_{SM}$  (*below*), as functions of the Higgs mass  $m_H$ . The results are obtained using a  $CL_s$  approach with a flat prior for the cross section, for 1.1 fb $^{-1}$ . Such limits are not sufficient to exclude the existence of the SM Higgs boson in the examined mass range. The same results for the SM augmented with a fourth generation of fermions with masses of 600 GeV/ $c^2$  are shown in Fig. 4 (*right*). The presence of another fermion family produces an enhancement of the dominant gluon-gluon fusion cross section. With 1.1 fb $^{-1}$ , Higgs masses in the range 250 – 560 GeV/ $c^2$  can be excluded in this model.

In this study, the exclusion limit is compared to the cross section for on-shell Higgs production and subsequent decay in the zero-width approximation. Acceptance estimates are obtained with Monte Carlo simulations based on ad-hoc Breit-Wigner distributions for describing the Higgs boson propagation. Recent analyses show that

Table III: Summary of the main systematic uncertainties affecting signal and background yields.

Source of uncertainty	Uncertainty [%]
Luminosity	6
PDF, gluon-gluon initial state	6-11
PDF, quark-quark initial state	3.3-7.6
QCD scale, gluon-gluon initial state	7.6-11 ( $ggH$ ), 20 ( $ggZZ$ )
QCD scale, quark-quark initial state	0.2-2 (VBF), 5.8-8.5 ( $qqVV$ )
Anti $b$ -tagging	1-1.2
Lepton ID, isolation	2
Lepton momentum scale	2 ( $2\mu$ ), 5 ( $2e$ )
Jet energy scale	1.5
Pileup	1-3
Trigger	2 ( $2\mu$ ), 1 ( $2e$ )
Non-resonant background estimation	15-100
Drell-Yan background estimation	51-54

Table IV: Expected number of signal and background events for an integrated luminosity of  $1.1 \text{ fb}^{-1}$  after full analysis selection, for dimuon (*above*) and dielectron (*below*) channels. Uncertainties for  $ZZ/WZ$  include the statistical and systematic components (in this order), non-resonant and  $Z$ +jets backgrounds have the full uncertainty quoted, and, finally, the signal column has only the systematic uncertainty quoted as the statistical uncertainty is negligible.

$m_H$	<b>ZZ</b>	<b>WZ</b>	<b>Non-resonant</b>	<b>Z + Jets</b>	<b>Total</b>	<b>Signal</b>	<b>Data</b>
250 $\text{GeV}/c^2$	$6.3 \pm 0.1 \pm 0.5$	$4.5 \pm 0.2 \pm 0.5$	$13 \pm 3$	$6.3 \pm 3.3$	$30 \pm 5$	$3.9 \pm 0.5$	28
300 $\text{GeV}/c^2$	$5 \pm 0.1 \pm 0.4$	$3.1 \pm 0.2 \pm 0.3$	$3 \pm 1.4$	$3.5 \pm 1.8$	$15 \pm 2$	$3.8 \pm 0.5$	13
350 $\text{GeV}/c^2$	$5.2 \pm 0.1 \pm 0.5$	$2.5 \pm 0.1 \pm 0.3$	$2 \pm 1.2$	$3.5 \pm 1.8$	$13 \pm 2$	$3.9 \pm 0.6$	11
400 $\text{GeV}/c^2$	$3.6 \pm 0.1 \pm 0.3$	$1.4 \pm 0.1 \pm 0.2$	$0.68 \pm 0.68$	$2.8 \pm 1.5$	$8.6 \pm 1.8$	$3.2 \pm 0.4$	6
500 $\text{GeV}/c^2$	$2 \pm 0.9 \pm 0.2$	$0.69 \pm 0.08 \pm 0.08$	0	$1.6 \pm 0.9$	$4.4 \pm 1$	$1.4 \pm 0.2$	3
600 $\text{GeV}/c^2$	$1.1 \pm 0.1 \pm 0.1$	$0.34 \pm 0.05 \pm 0.04$	0	$1 \pm 0.5$	$2.5 \pm 0.7$	$0.57 \pm 0.08$	2

$m_H$	<b>ZZ</b>	<b>WZ</b>	<b>Non-resonant</b>	<b>Z + Jets</b>	<b>Total</b>	<b>Signal</b>	<b>Data</b>
250 $\text{GeV}/c^2$	$4.6 \pm 0.1 \pm 0.5$	$3.6 \pm 0.2 \pm 0.4$	$9.4 \pm 2.2$	$4 \pm 2.1$	$22 \pm 5$	$3.1 \pm 0.4$	29
300 $\text{GeV}/c^2$	$3.8 \pm 0.1 \pm 0.4$	$2.2 \pm 0.1 \pm 0.3$	$2.2 \pm 1$	$2.6 \pm 1.3$	$11 \pm 3$	$3.1 \pm 0.4$	21
350 $\text{GeV}/c^2$	$4.2 \pm 0.1 \pm 0.4$	$1.8 \pm 0.1 \pm 0.2$	$1.3 \pm 0.8$	$3.2 \pm 1.7$	$11 \pm 3$	$3.2 \pm 0.5$	8
400 $\text{GeV}/c^2$	$3 \pm 0.1 \pm 0.3$	$1.2 \pm 0.1 \pm 0.1$	$0.5 \pm 0.5$	$2.6 \pm 1.3$	$7.3 \pm 2$	$2.5 \pm 0.3$	7
500 $\text{GeV}/c^2$	$1.6 \pm 0.1 \pm 0.2$	$0.62 \pm 0.07 \pm 0.07$	0	$1.7 \pm 0.9$	$3.9 \pm 1.2$	$1.1 \pm 0.2$	2
600 $\text{GeV}/c^2$	$0.97 \pm 0.06 \pm 0.09$	$0.31 \pm 0.05 \pm 0.04$	0	$1 \pm 0.6$	$2.3 \pm 0.7$	$0.47 \pm 0.07$	1

the use of a QFT-consistent Higgs propagator, and allowing for the off-shellness of the Higgs boson, dynamical QCD scales, and interference effects between Higgs signal and backgrounds, will result, at Higgs masses above 300  $\text{GeV}/c^2$ , in a sizable effect on conventionally defined but theoretically consistent parameters (mass and width) that describe the propagation of an unstable Higgs boson [4, 20, 21]. In this work, these effects are included as an additional uncertainty of 10-30% (for 400 to 600  $\text{GeV}/c^2$  Higgs mass) on the theoretical cross section.

## Acknowledgments

The author would like to thank the CMS Higgs PAG conveners, professors Vivek Sharma and Christoph Paus; the conveners of the HZZ subgroup, Dr. Chiara Mariotti and Prof. Ivica Puljak; and the whole HZZ212nu working group, especially Adish Vartak, Dr. Alexey Drozdetskiy and Dr. Petra Merkel, for coordinating the huge effort that has led to the results here presented.

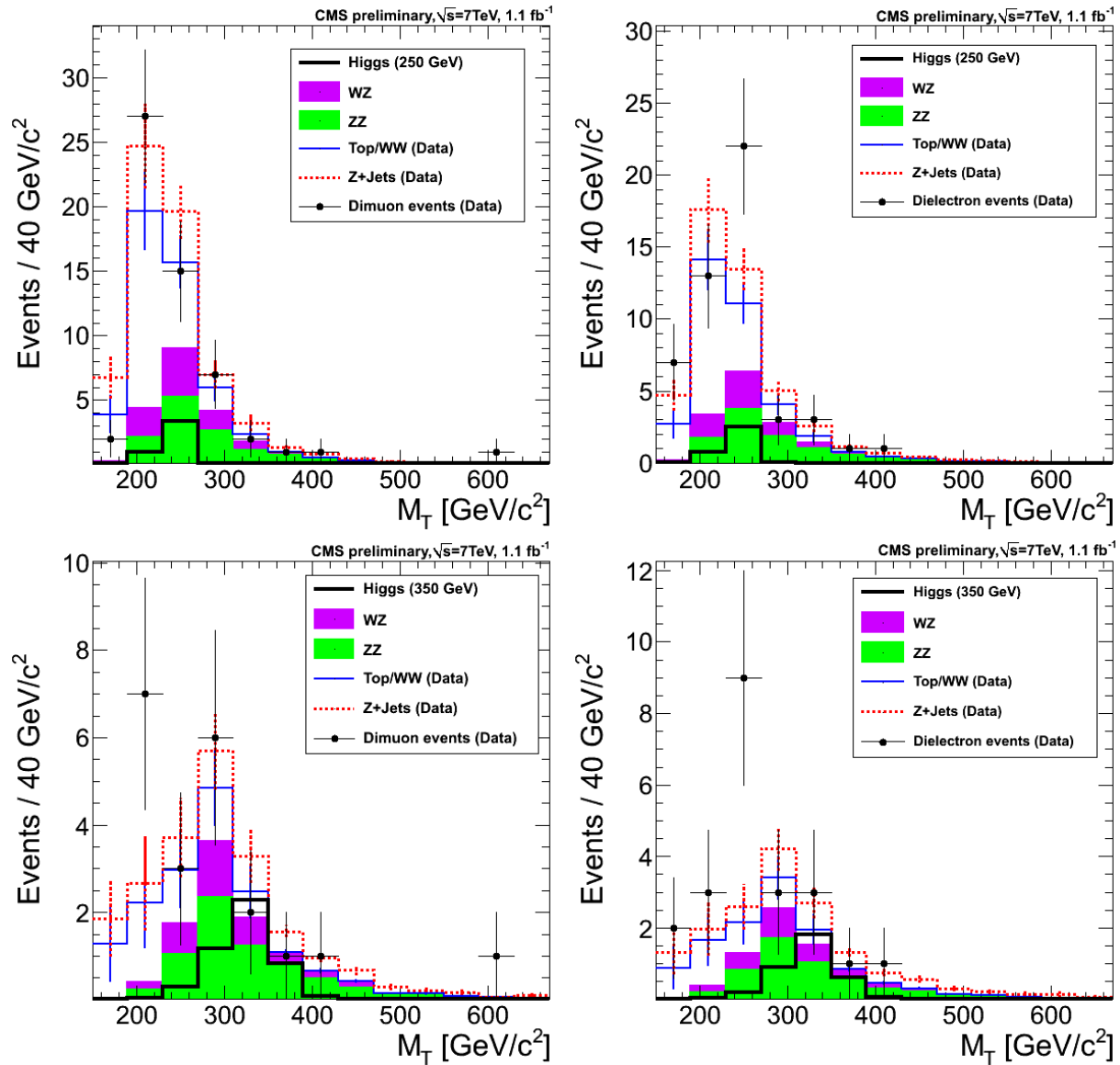


Figure 3:  $M_T$  distribution of events passing the 250  $\text{GeV}/c^2$  (above) and 350  $\text{GeV}/c^2$  (below) Higgs mass selections, in the muon (left) and electron (right) channels.

## References

- 1 ALEPH, DELPHI, L3, OPAL Collaborations, LEP Working Group for Higgs boson searches, "Search for the Standard Model Higgs boson at LEP", *Phys. Lett. B* **505** (2003) 61.
- 2 CDF, D0 Collaborations, TEVNPHWG Working Group, "Combined CDF and D0 Upper Limits on Standard Model Higgs Boson Production with up to 8.2  $\text{fb}^{-1}$  of Data", arXiv:1103.3233v2.
- 3 CMS Collaboration, "Search for the Higgs boson in the  $H \rightarrow ZZ \rightarrow 2l2\nu$  channel in pp collisions at  $\sqrt{s} = 7$  TeV", CMS-PAS-HIG-11-005 (2011).
- 4 LHC Higgs Cross Section Working Group, S. Dittmaier, C. Mariotti *et al.*, "Handbook of LHC Higgs Cross Sections: 1. Inclusive Observables", CERN-2011-002 (CERN, Geneva, 2011) arXiv:1101.0593.
- 5 Q. Li, M. Spira, J. Gao, C.S. Li, "Higgs boson production via gluon fusion in the standard model with four generations", arXiv:1011.4484 (2010).
- 6 T. Aaltonen *et al.*, "Combined Tevatron upper limit on  $gg \rightarrow H \rightarrow W^+W^-$  and constraints on the Higgs boson mass in fourth-generation fermion models", *Phys. Rev. D* **82** (2010) 011102.
- 7 CMS Collaboration, "The CMS experiment at the CERN LHC", *JINST* **3** (2008) S08004.

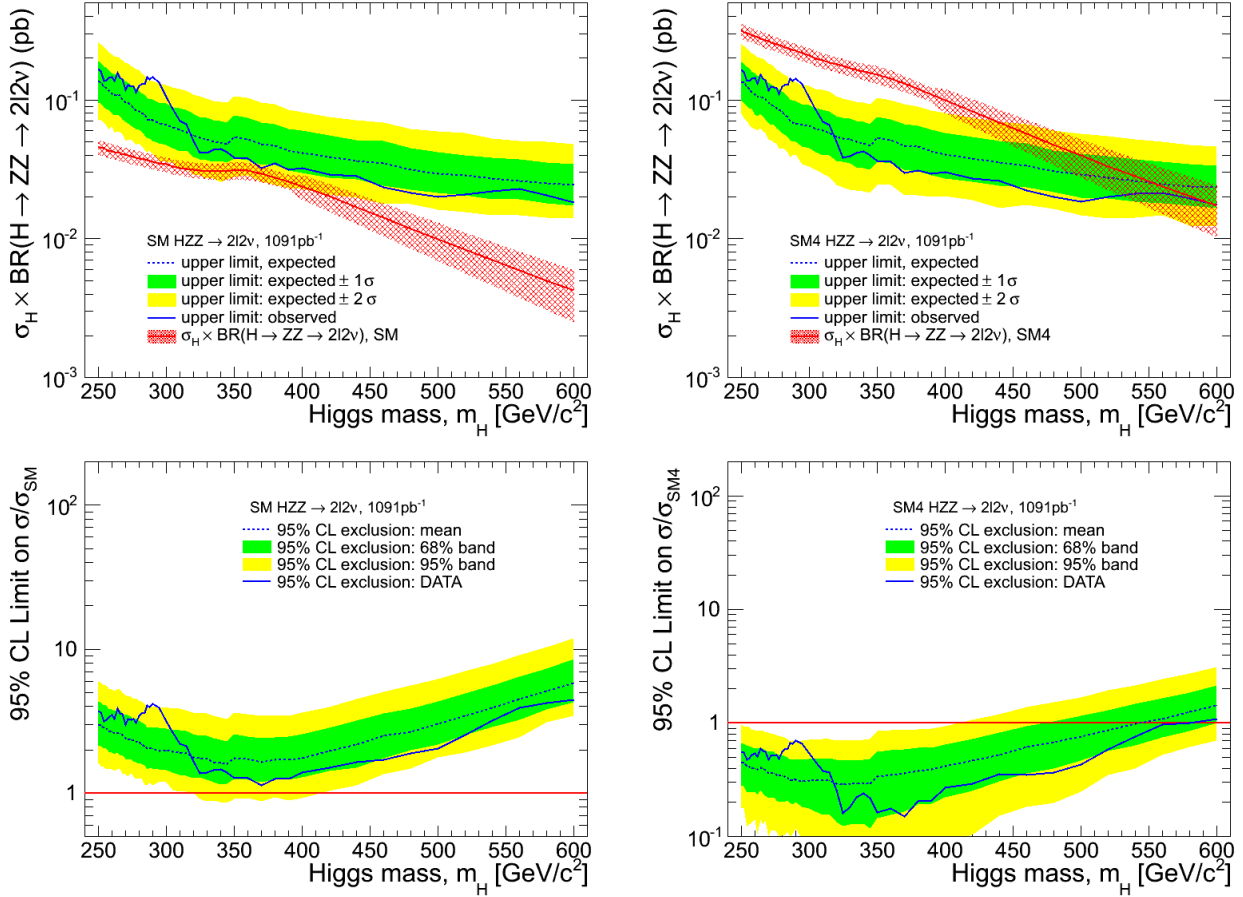


Figure 4: *Above*: 95% mean expected and observed C.L. upper limits on the  $H \rightarrow ZZ \rightarrow 2\ell 2\nu$  cross section (in red), in the SM (*left*) and SM + 4<sup>th</sup> generation (*right*). *Below*: ratio of the 95% C.L. upper limit ( $\sigma$ ) to the SM cross section  $\sigma_{SM}$  (*left*), and SM + 4<sup>th</sup> generation cross section  $\sigma_{SM4}$ . All results are relative to 1.1 fb<sup>-1</sup> of integrated luminosity.

- 8 S. Agostinelli *et al.*, “Geant 4 A Simulation Toolkit”, *Nucl. Inst. Meth. A* **506** (2003) 250.
- 9 S. Frixione, P. Nason, C. Oleari, “Matching NLO QCD computations with Parton Shower simulations: the POWHEG method”, *JHEP* **11** (2007) 070, [arXiv:0709.2092](#).
- 10 F. Maltoni, T. Stelzer, “MadEvent: Automatic event generation with MadGraph”, *JHEP* **02** (2003), [arXiv:0208156](#).
- 11 T. Sjöstrand, S. Mrenna, P. Skands, “PYTHIA 6.4 physics and manual”, *JHEP* **05** (2007).
- 12 J. M. Campbell, R. K. Ellis, “MCFM for the Tevatron and the LHC”, [arXiv:1007.3492](#).
- 13 T. Binoth, N. Kauer, P. Mertsch, “Gluon-induced QCD corrections to  $pp \rightarrow ZZ \rightarrow l \text{ anti-}l' l' \text{ anti-}l'$ ”, [arXiv:0807.0024](#).
- 14 CMS Collaboration, “Performance of muon identification in 2010 data”, **CMS-PAS-MUO-10-004** (2010).
- 15 CMS Collaboration, “Electron reconstruction and identification at  $\sqrt{s} = 7$  TeV”, **CMS-PAS-EGM-10-004** (2010).
- 16 M. Cacciari, G. P. Salam, G. Soyez, “The Catchment Area of Jets”, *JHEP* **04** (2008) 005, [arXiv:0802.1188](#).
- 17 CMS Collaboration, “Jet Performance in pp Collisions at  $\sqrt{s} = 7$  TeV”, **CMS-PAS-JME-10-003** (2010).
- 18 CMS Collaboration, “Performance of b-jet identification in CMS”, **CMS-PAS-BTV-11-001** (2011).
- 19 CMS Collaboration, “MET Performance in Events Containing Electroweak Bosons from pp Collisions at  $\sqrt{s} = 7$  TeV”, **CMS-PAS-JME-10-005** (2010).
- 20 C. Anastasiou, S. Buehler, F. Herzog *et al.*, “Total cross-section for Higgs boson hadroproduction with anomalous Standard Model interactions”, [arXiv:1107.0683](#).
- 21 G. Passarino, C. Sturm, S. Uccirati, “Higgs Pseudo-Observables, Second Riemann Sheet and All That”, *Nucl. Phys.* **B834** (2010) 77-115, [arXiv:1001.3360](#).